

# Bayesian Learning for Dynamic Target Localization with Human-provided Spatial Information

Min-Won Seo<sup>1</sup> and Solmaz S. Kia<sup>1</sup>, *Senior Member, IEEE*

**Abstract**—This paper considers a human-autonomy collaborative sensor data fusion for dynamic target localization in a Bayesian framework. To compensate for the shortcomings of an autonomous tracking system, we propose to collect spatial sensing information from human operators who visually monitor the target and can provide target localization information in the form of free sketches encircling the area where the target is located. Our focus in this paper is to construct an adaptive probabilistic model for human-provided inputs where the adaption terms capture the level of reliability of the human inputs. The next contribution of this paper is a novel joint Bayesian learning method to fuse human and autonomous sensor inputs in a manner that the dynamic changes in human detection reliability are also captured and accounted for. A unique aspect of this Bayesian modeling framework is its analytical closed-form update equations, endowing our method with significant computational efficiency. Simulations demonstrate our results.

## I. INTRODUCTION

Dynamic target localization using sensor measurements collected by autonomous agents has been of interest for a long time. Multi-agent target localization where multiple agents from different perspectives obtain measurements from the target and fuse them together has demonstrated an improvement in accuracy [1]–[3]. Despite advances in sensor data fusion algorithms and autonomous perception abilities, relying merely on the hard sensor measurements collected by only the autonomous sensors does not always result in an acceptable level of localization accuracy in complex environments. This is because autonomous sensors can suffer from observability and target recognition failures, see Fig. 1. Recently, including human observers that can provide spatial information to localize dynamic targets in challenging environments has been proposed to compensate for the shortcomings of the autonomous sensors [4]–[7]. This has resulted in effective tracking and localization of the target in time-critical tasks.

Humans possess valuable qualitative information derived from their past knowledge and rapid situational awareness that can give them an advantage over machine perception in many scenarios. However, it is essential to admit that the sensory inputs provided by humans are inherently subjective and “soft” in nature [8]. Humans are prone to making mistakes, and their abilities can vary depending on the situation, prior experience, and even the current state of mind. Consequently, excessive reliance on human input can lead to poor performance and should be avoided [9]. It is critical to have a proper *mathematical model* for quantifying human inputs to ensure the success and effectiveness of



Fig. 1 – Examples of the machine learning-based object detection algorithm (YOLO [10]) failure to detect (a person on the left figures) or miss-detect (a drone on the right figure). (Left) The initial correct detection is compromised due to intense sun glare. (Right) Detection falters due to a complex background and insufficient data. In both these examples, a human can readily identify the targets, providing valuable assistance to tracking systems.

human-autonomous collaboration for localization. The model should consider uncertainty factors such as human reliability (errors). Additionally, model parameters need to be updated online to capture changes in the uncertainty of human reliability over time. By considering these aspects, we can build estimation pipelines that enable efficient integration of human input, thus facilitating improved localization outcomes in cooperative human-autonomous systems.

In recent years, human-autonomy collaborative sensor data fusion has played a significant role in various sensing and planning tasks. For example, in [11], [12], qualitative spatial constraints for manipulators are acquired from human spoken commands. However, variations in human pronunciation and ambient noise levels can impact the system’s effectiveness. On the other hand, [13] proposes a fusion of human electroencephalography (EEG) and autonomic sensor data, thus requiring additional hardware and accounting for EEG sensitivity to external interference. [14] primarily focuses on human-assisted site inspection tasks aimed at addressing real wireless communication, rather than emphasizing human information expression. In [15], the authors present a method to detect and track targets from a human perspective using a headset, which might be affected by the human’s field of view. These studies highlight the valuable contributions of human-provided information in collaborative tasks that cannot be obtained solely from autonomous systems. In this paper, our focus is on the use of human sketch-based spatial localization in dynamic target tracking.

In dynamic target localization, sensor information plays a crucial role in continuously tracking the target. Additionally, the information should be presented in a clear way (reduced language barriers) and concisely (data compression). Leveraging drawing-type observations as a semantic language interface presents potential advantages. Firstly, it can be readily applied to widely used mobile systems such as smart-

<sup>1</sup>Min-Won Seo, and Solmaz S. Kia are with the Department of Mechanical and Aerospace Engineering, University of California, Irvine, CA 92697, USA, {minwons, kia}@uci.edu

phones, tablets, and emerging technologies like Augmented Reality (AR) and Virtual Reality (VR). Secondly, drawing-based information is highly intuitive and practical for both robots and humans. However, the observation model must proficiently capture human reliability *without* imposing a computational burden while delivering accurate information. Research on human drawing information fusion is conducted within robotics applications [16]–[18]. The authors of [16] illustrate humans conveying map data via hand-sketched drawings for robot navigation, however, neglect inherent human-provided information uncertainty. In contrast, [17] presents a human sketch-based method for static target search with uncertainty, but it doesn't consider the computational costs of parameter updates. The authors of [18] place their primary emphasis on online planning using human drawing observations, rather than focusing on the updating of human parameters.

This paper introduces a novel human drawing model incorporating uncertainty for dynamic target localization, emphasizing the importance of computational efficiency in updating the distribution of human parameters (detection reliability). Especially, the distribution of human parameters is updated in the *closed* form through Bayesian learning, enabling real-time tracking tasks. The main contributions of this paper are

- We present a novel probabilistic observation model for human drawings that considers not only the reliability of human detection but also incorporates inherent uncertainty. Moreover, its conjugate closed-form structure enhances computational efficiency, a crucial factor in dynamic target localization.
- We propose a joint Bayesian learning approach that concurrently operates target localization and updates human parameters. This strategy enables online adjustments of human parameters to precisely depict the evolving human detection reliability over time.
- We demonstrated improved target localization results and the updated distribution of human detection reliability in a simulation study.

The remainder of this paper is organized as follows: Section II presents the problem definition. Section III describes the particle-based target localization framework. In Section IV, we present our novel human-drawing observation likelihood model, which incorporates human detection reliability and facilitates sensor data fusion. Furthermore, in Section V, we discuss joint Bayesian learning for target localization and human parameters. Section VI reports the simulation results. Finally, Section VII gives the conclusion.

## II. PROBLEM DEFINITION

This paper considers a dynamic target localization problem where a team of autonomous sensors  $u \in \mathcal{U} = [u_1, \dots, u_n]^T$  with help from human operators  $h \in \mathcal{H} = [h_1, \dots, h_m]^T$  estimate the location of a mobile target, see Fig 2. The target moves on a 2D terrain  $\Theta \subset \mathbb{R}^2$ . The sensors using e.g., a stereo camera with a limited field of view, provide image data of the target and relative range information between the target and themselves; measurements can also be other types of observations, e.g., bearing measurement. We assume that real-time, possibly low-resolution, footage of the target obtained e.g., a UAV flying over the scene is streamed for human observers [19]. Human operators

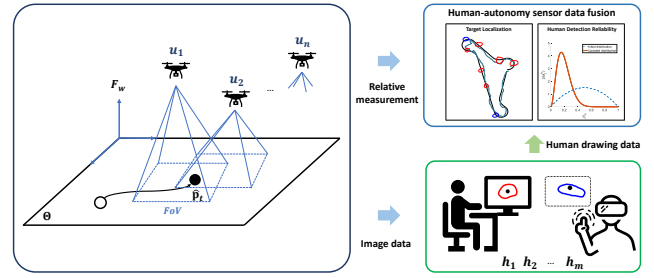


Fig. 2 – A representative scenario of the problem of interest in this paper: A target, depicted by  $\bullet$ , moves in a 2D space. UAVs equipped with a stereo vision camera transmit relative measurements to a centralized fusion center, and image data to human operators. The human operators provide inside drawing observations on the image data via a touch screen monitoring system (e.g., tablet). The human and autonomous sensor data fusion is performed to localize the target in the centralized system.

offer spatial sensing about the target's location based on their visual perception of the image data by enclosing the location of the target on the image plane. The observations are transmitted to a centralized system for integrating data and estimating the target position. It is assumed that there is no exchange of information among team members, thus there is no conditional dependency between the sensors and human observers.

Let the position of the target at time  $t$  be denoted by  $\mathbf{p}_t = [x \ y]^T \in \Theta$ , where  $x$  and  $y$  represent its 2D coordinates at time index  $t$  in a 3D world frame  $\mathcal{F}_w \subset \mathbb{R}^3$ . When the target position vector is expressed in the 3D coordinate, it is represented as  $\mathbf{p}_t^+ = [\mathbf{p}_t^T \ 0]^T$ . The state of the sensing platform  $u$  is the camera pose  $\mathbf{s}_{u,t} = [\mathbf{c}_{u,t}^T \ \psi_{u,t}]^T$ , where  $\mathbf{c}_{u,t} \in \mathbb{R}^3$  is the position of the sensor, referred to  $\mathcal{F}_w$ , and  $\psi_{u,t} \in [0, 2\pi]$  is the yaw angle of the sensing platform. We assumed image data is obtained in the face-down view [20], however, it can be extended to any view of the image data. Our objective is to estimate the position of the target, denoted by  $\hat{\mathbf{p}}_t$ , by integrating observations from autonomous sensors'  $u \in \mathcal{U}$  and human operators'  $h \in \mathcal{H}$  drawing-based observations.

## III. TARGET LOCALIZATION FRAMEWORK

This section presents our Bayesian target localization framework that enables fusing human and autonomous sensor measurements to localize the target described in Section II. The likelihood model for range observation from autonomous sensors is a non-linear function of the target state, see Section III-D, and human observations, as will be shown in Section IV, is a non-Gaussian model, resulting in complex posterior distributions. To solve our problem, thus, we propose to use a finite-state Hidden Markov Model (HMM) based framework. This non-parametric Bayesian framework offers the advantage of expressing probabilities explicitly using a discrete sample space, enabling recursive Bayesian inference in *closed* form. Additionally, it seamlessly incorporates geometric information, such as barriers or boundaries, into localization [21]. Furthermore, integration with the control and planning pipeline is readily achieved, as finite state-based techniques commonly establish action (control) policies [22], [23].

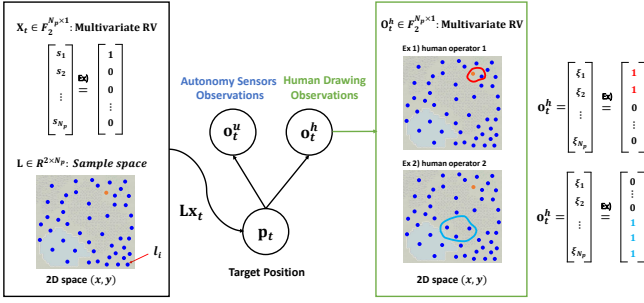


Fig. 3 – Target localization via Hidden Markov Model.  $\mathbf{X}_t \in \mathbb{F}_2^{N_p \times 1}$  represents a multivariate random variable (random vector) at every time step. Each element  $s_i$  of  $\mathbf{X}_t$  is mapped into the particle  $\mathbf{l}_i$  in 2D sample space  $\mathbf{L} \in \mathbb{R}^{2 \times N_p}$ . Therefore, the position of the target  $\mathbf{p}_t \in \Theta$  is computed by  $\mathbf{L}\mathbf{x}_t$ . There is human-drawing observation  $\mathbf{O}_t^h \in \mathbb{F}_2^{N_p \times 1}$ , indicating the target inside. In this example, two human operators draw the region, where, unlike  $\mathbf{X}_t$  that only has a single  $s_i = 1$ ,  $\mathbf{O}_t^h$  can have multiple  $\zeta_j = 1$ .

#### A. Hidden Markov Model Framework

We discretize the target workspace via  $N_p$  particles which generate a 2D sample space  $\mathbf{L} = [\mathbf{l}_1, \dots, \mathbf{l}_{N_p}] \in \mathbb{R}^{2 \times N_p}$  where  $\mathbf{l}_i = [x \ y]^\top \in \Theta$  is the position of  $i$ -th particle and  $N_p$  is the total number of particles, see Fig 3. The particles can be positioned within areas that align with the target's possible movement based on map information, such as roads.

The HMM has two stochastic processes, hidden states,  $\mathbf{x}_t \in \mathbf{X}_t$ , and observations,  $\mathbf{o}_t^u \in \mathbf{O}_t^u$ ,  $\mathbf{o}_t^h \in \mathbf{O}_t^h$  at each time step  $t$ . The hidden state encapsulates the belief regarding the target's position within a discretized sample space. Observations are obtained from autonomous sensors and human operators. The hidden state  $\mathbf{x}_t$  takes values from  $\mathbf{X}_t = [s_1, s_2, \dots, s_{N_p}]^\top \in \mathbb{F}_2^{N_p \times 1}$  where  $s_i$  takes the binary number 1 or 0. Each element  $s_i$  is mapped one-to-one into the particle  $\mathbf{l}_i$  in the particle-based sample space. Since we are localizing only one target,  $\mathbf{X}_t$  can have *only one*  $s_i = 1$ , and *all the other elements are set to*  $s_j = 0$ ,  $j \neq i$ . Therefore multiplication  $\mathbf{L}\mathbf{x}_t$  corresponds to the position of the target  $\mathbf{p}_t$  ( $\mathbf{p}_t = \mathbf{L}\mathbf{x}_t$ ). While autonomous sensors' range observation  $\mathbf{o}_t^u$  can take real values  $\mathbf{O}_t^u \in \mathbb{R}_{\geq 0}$ , human-drawing observation  $\mathbf{o}_t^h$  takes values from  $\mathbf{O}_t^h = [\zeta_1, \zeta_2, \dots, \zeta_{N_p}]^\top$ ,  $\mathbf{O}_t^h \in \mathbb{F}_2^{N_p \times 1}$  where  $\zeta_i$  takes the binary number 1 or 0. Unlike  $\mathbf{X}_t$ , which only has a single  $s_i = 1$  at each time step,  $\mathbf{O}_t^h$  can have *multiple*  $\zeta_j = 1$ , as depicted in Fig 3. Therefore, it is important to carefully quantify the information between  $\mathbf{X}_t$  and  $\mathbf{O}_t^h$ . It will be thoroughly discussed in Section IV.

#### B. The Forward Algorithm for Recursive Bayesian Filtering

To estimate the target's 2D position (state) at time step  $t$  from all the observations, denoted by  $\{\mathbf{o}_{1:t}^u, \mathbf{o}_{1:t}^h\} \subset \mathbf{o}_{1:t}$ , we propose to use a recursive Bayesian approach. Our goal is to find the posterior distribution of the target's state,

$$p(\mathbf{p}_t | \mathbf{o}_{1:t}) = \eta p(\mathbf{o}_t | \mathbf{p}_t) \int_{\Theta} p(\mathbf{p}_t | \mathbf{p}_{t-1}) p(\mathbf{p}_{t-1} | \mathbf{o}_{1:t-1}) d\mathbf{p}_{t-1}, \quad (1)$$

where  $\eta$  is a normalizing constant that ensures the posterior adds up to 1. A prior distribution  $p(\mathbf{p}_0)$  is constructed from any information available a prior. Here,  $p(\mathbf{p}_{t-1} | \mathbf{o}_{1:t-1})$  is a

posterior distribution at the previous step  $t-1$ ,  $p(\mathbf{p}_t | \mathbf{p}_{t-1})$  is a Markovian state transition model for the target (for details see Section III-C). The integral term is from Chapman-Kolmogorov equation [24].  $p(\mathbf{o}_t | \mathbf{p}_t)$  is an observation model (those are referred to as likelihood function in the probabilistic form) that will be discussed in III-D and IV. The likelihood model for range observation is a non-linear function of the target state and for human observation is a non-Gaussian model, resulting in complex posterior distributions. The HMM approach can handle these issues by obtaining non-parametric posterior distributions.

HMM-based estimators can be designed to estimate either the joint probability,  $p(\mathbf{x}_{1:t} | \mathbf{o}_{1:t})$ , or the marginal probability,  $p(\mathbf{x}_t | \mathbf{o}_{1:t})$ . Here, given the 2D sample space  $\mathbf{L}$ , we can calculate  $p(\mathbf{p}_{1:t} | \mathbf{o}_{1:t})$  and  $p(\mathbf{p}_t | \mathbf{o}_{1:t})$  from  $p(\mathbf{x}_{1:t} | \mathbf{o}_{1:t})$  and  $p(\mathbf{x}_t | \mathbf{o}_{1:t})$ , respectively. Several well-known HMM-based algorithms exist, including the forward, forward-backward, and Viterbi algorithms [25]. In this paper, we employ the forward algorithm to recursively estimate the distribution of the most probable position denoted by  $p(\mathbf{p}_t | \mathbf{o}_{1:t})$  at each time step  $t$ . The forward algorithm shares similarities with the Kalman filter, as it involves prediction and correction steps. However, the fundamental distinction lies in the nature of the sample space, which is discrete (finite) rather than continuous (infinite). As a result, the integral term and  $\eta$  in equation (1) can be calculated through summation. The posterior distribution of target locations can be represented in discrete form as given by

$$p(\mathbf{p}_t | \mathbf{o}_{1:t}) \approx \sum_{i=1}^{N_p} q_t^i \cdot \delta(\mathbf{p}_t - \mathbf{p}_t^i), \quad (2)$$

where  $\delta(\cdot)$  is the Dirac delta function, and  $q_t^i$  is the weight for the  $i^{th}$  target location  $\mathbf{p}_t^i$  and satisfied with  $\sum_{i=1}^{N_p} q_t^i = 1$ . Subsequently, the minimum mean square error (MMSE) estimate of the position of the target is computed from

$$\hat{\mathbf{p}}_t = \int_{\Theta} \mathbf{p} \cdot p(\mathbf{p}_t | \mathbf{o}_{1:t}) d\mathbf{p} \approx \sum_{i=1}^{N_p} \mathbf{p}_t^i \cdot q_t^i \cdot \delta(\mathbf{p}_t - \mathbf{p}_t^i). \quad (3)$$

#### C. The Transition Model for a Model-free Target

Our problem setting considers scenarios where we have no access to proprioceptive sensors to perform dead-reckoning to predict target movement from its model. That is, we consider a target-tracking problem where the motion of the target is not parameterized. To localize such targets, we use a constant velocity motion model that is widely used in tracking problems [26]–[28] as follows

$$p(\mathbf{p}_t | \mathbf{p}_{t-1}) = \mathcal{N}(\mathbf{p}_t; \mathbf{p}_{t-1} + \mathbf{v}_{t-1} T_s, \frac{T_s^2}{2} \sigma_p^2 \mathbf{I}), \quad (4)$$

where

$$\mathbf{v}_t \sim \mathcal{N}(\mathbf{v}_t; \mathbf{v}_{t-1}, T_s \sigma_p^2 \mathbf{I}), \quad (5)$$

where  $\sigma_p \in \mathbb{R}_{>0}$  denotes the standard deviation in the assumed constant velocity motion model at time step  $t$ ,  $\mathbf{I}$  is the identity matrix according to dimension, and  $\mathcal{N}(x; \mu, \Sigma)$  is a Gaussian with mean  $\mu$  and covariance  $\Sigma$ .  $T_s$  is the inter-sampling time and  $\mathbf{v}_t = [v_x \ v_y]^\top \in \mathbb{R}^2$  is the constant velocity of the target with predefined  $\mathbf{v}_0$ .

#### D. The Likelihood Model for Autonomous Sensor

The target is detected in the image data through a vision-based detection algorithm [10], [29], [30]. The sensing platform  $u$  computes the relative distance via image data using a stereo camera [31]. The likelihood model for the distance information of sensor  $u$  is

$$p(\mathbf{o}_t^u | \mathbf{p}_t) = \mathcal{N}(\mathbf{o}_t^u; r_t, \sigma_d^2) \Gamma(D_t | p_d), \quad (6)$$

where  $r_t = \|\mathbf{c}_{u,t} - \mathbf{p}_t^+\|_2 \in \mathbb{R}_{\geq 0}$  is the range between the position of the sensor platform  $\mathbf{c}_{u,t}$  and the position of the target  $\mathbf{p}_t^+$ . To represent the uncertainties in range observations, we incorporate the Gaussian noise assumption in the sensor model. In addition, we simplify the detection event by using a Bernoulli random variable. This random variable takes into account whether the target is successfully detected or not by the sensor. The success probability of detection, denoted by  $p_d$ , represents the likelihood of a successful detection event by

$$\Gamma(D_t | p_d) = \begin{cases} 1, & D_t = 1 \quad (\text{detected}) \\ 0, & D_t = 0 \quad (\text{undetected}) \end{cases} \quad (7)$$

#### IV. THE HUMAN DRAWING LIKELIHOOD MODEL

For human-drawing spatial observations, we consider inside-drawing observations indicating that the target is inside (refer to Fig 3). Assuming the human drawing is a simplex closed-area shape, the drawing on the visual interface plane (e.g., tablet) is approximated as a set of finite distinct points. Then, these points are transformed into the 2D plane  $\Theta$  using a rotation matrix  $\mathbf{R}_w^c(\psi_{u,t})$  and the camera intrinsic parameter matrix  $\mathbf{K}$  [31]. This transformation enables the calculation of the likelihood in the 2D space  $\Theta$ .

Human detection capability to recognize the target in the image varies from person to person. Even for each person, this ability can change depending on the person's state of mind, workload, and environmental factors. The human likelihood model we propose captures this detection reliability and changes in the reliability of human operators over time.

##### A. Human Detection Reliability

To design the human likelihood model, we represent human detection reliability for human-drawing observations as conditional probability. Let's consider the *ground truth* state of the target,  $\mathbf{x}_t^g \in \mathbf{X}_t$ , and the human drawing observation  $\mathbf{o}_t^h \in \mathbf{O}_t^h$ . Given the *ground truth* target state  $\mathbf{x}_t^g$ , the probability of the inside drawing observation can be expressed by

$$p(\mathbf{O}_t^h = \mathbf{o}_t^h | \mathbf{X}_t = \mathbf{x}_t^g) = \begin{cases} a_t^h, & \mathbf{o}_t^h = \mathbf{x}_t^g \quad (\text{true}) \\ 1 - a_t^h, & \mathbf{o}_t^h \neq \mathbf{x}_t^g \quad (\text{false}) \end{cases}, \quad (8)$$

where  $a_t^h \in [0, 1] \subseteq \mathbb{R}$  indicates human detection reliability at time  $t$ . The conditional probability, represented as  $a_t^h$  (true inside), indicates the possibility of a match between the true state  $\mathbf{x}_t^g$  and the observation  $\mathbf{o}_t^h$ . Conversely, if there is no match, the probability is expressed as  $1 - a_t^h$  (false inside).

A high value of  $a_t^h$  indicates strong trust in human input (high reliability), and conversely, a low value indicates less trust (low reliability). However, human abilities are different from person to person, and can also change during the course

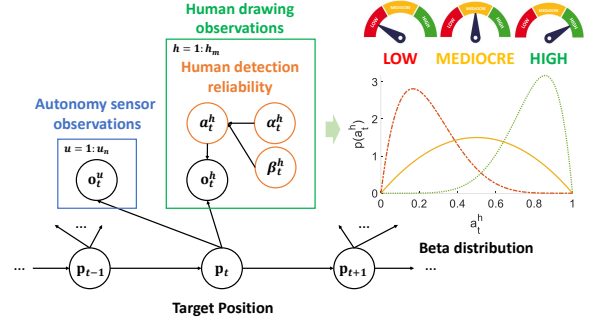


Fig. 4 – Probabilistic graph model for human-autonomy collaborative sensor data fusion.  $\mathbf{p}_t$  is the position of a target at a given time  $t$ . Autonomy sensors observations  $\mathbf{o}_t^u \in \mathbf{O}_t^u$  are obtained from mobile agents  $u \in \mathcal{U}$  at a given time  $t$ . Human-drawing observations  $\mathbf{o}_t^h \in \mathbf{O}_t^h$  are provided by human operators  $h \in \mathcal{H}$  at a given time  $t$ . At time index  $t$ , the human  $h$ 's detection reliability for drawing observations is represented as  $a_t^h \sim \text{Beta}(\alpha_t^h, \beta_t^h)$ . By using different values for  $\alpha_t^h$  and  $\beta_t^h$ , we can capture various levels of reliability.

of an operation. Therefore, instead of using a predetermined fixed value, we model  $a_t^h$  as a probabilistic distribution, the parameters of which are learned online.

To quantify the uncertainty of the human detection reliability, we apply a Bayesian approach of  $a_t^h$  by modeling it with a Beta distribution,

$$a_t^h \sim \text{Beta}(\alpha_t^h, \beta_t^h), \quad (9)$$

where  $\alpha_t^h \in \mathbb{R}_{>0}$  and  $\beta_t^h \in \mathbb{R}_{>0}$  are the parameters of the distribution at time  $t$ . The beta distribution, defined within the interval  $[0, 1] \subseteq \mathbb{R}$ , is well-suited for statistical modeling of human detection reliability and has been previously used in other contexts such as human-aided text classification [32]. For different values of  $\alpha_t^h$  and  $\beta_t^h$ , we can capture different levels of reliability as shown in Fig 4 on the right (low, mediocre, high). For simple notation, we will omit the subscript  $h$  from  $\alpha_t^h$  and  $\beta_t^h$ , except when it is necessary. We will learn these parameters as part of our Bayesian fusion method.

##### B. The Likelihood Model for Human Drawing Observations

Based on the human detection reliability  $a_t^h$ , we propose a likelihood function for human-drawing observations. Initially, we will focus on  $\mathbf{o}_t^h$ , where 'only one' element  $\zeta_i$  is set to 1, while all other elements  $\zeta_j$  are set to 0 ( $j \neq i$ ). Given  $\mathbf{X}_t = \mathbf{x}_t$ , the likelihood function for inside drawing  $\mathbf{o}_t^h$  of human operator  $h$  can be expressed using the Kronecker delta function  $\delta(\cdot, \cdot)$  by

$$p(\mathbf{o}_t^h | \mathbf{x}_t, a_t^h; \mathbf{L}) = (a_t^h)^{\delta(\mathbf{x}_t, \mathbf{o}_t^h)} \times (1 - a_t^h)^{(1 - \delta(\mathbf{x}_t, \mathbf{o}_t^h))}, \quad (10)$$

where  $\delta(\mathbf{x}_t, \mathbf{o}_t^h) = 1$  if  $\mathbf{x}_t = \mathbf{o}_t^h$ , and  $\delta(\mathbf{x}_t, \mathbf{o}_t^h) = 0$  otherwise. The likelihood function can be interpreted as representing the probability of successful human detection for a single enclosed particle.

Next, we extend our consideration to include 'multiple'  $\zeta_i = 1$  in  $\mathbf{o}_t^h$  (e.g.,  $\mathbf{o}_t^h = [1, 1, 0, \dots, 0]^T$ ). Let's define a set  $\mathcal{O}_t = \{[\xi_1, \xi_2, \dots, \xi_{N_p}]^T \in \mathbb{F}_2^{N_p \times 1} \mid \sum_{i=1}^{N_p} \xi_i =$

$1, i \in \{1, \dots, N_p\}\}$ . When the human drawing observation  $\mathbf{o}_t^h$  contains  $M$  number of  $\zeta_i = 1$ , there exists a subset  $\mathcal{S}_t^M \subseteq \mathcal{O}_t$  with  $M$  elements. For example, in the case of  $N_p = 3$ , the set  $\mathcal{O}_t$  can be represented as  $\mathcal{O}_t = \{[1, 0, 0]^\top, [0, 1, 0]^\top, [0, 0, 1]^\top\}$ . If the human drawing observation is  $\mathbf{o}_t^h = [1, 1, 0]^\top$ , the corresponding subset would be  $\mathcal{S}_t^M = \{[1, 0, 0]^\top, [0, 1, 0]^\top\}$ . Here, we assume no correlation between elements within the subset  $\mathcal{S}_t^M$  (i.e., the naive Bayes assumption [25]). Then,  $\mathcal{S}_t^M$  can be interpreted in two possibilities; the target may be located here, and it may not be located here. Consequently, assuming that when humans draw regions of space, particles are selected independently in a sequential manner, the likelihood function for the inside drawing can be represented using the rule of the product,

$$\begin{aligned} p(\mathbf{o}_t^h | \mathbf{x}_t, a_t^h; \mathbf{L}) &= \prod_{\forall \mathbf{o}_t^M} l(\mathbf{o}_t^M | \mathbf{x}_t, a_t^h; \mathbf{L}) \\ &= (a_t^h)^{\delta(\mathbf{x}_t, \mathbf{o}_t^M)} \times (1 - a_t^h)^{(M - \delta(\mathbf{x}_t, \mathbf{o}_t^M))}, \end{aligned} \quad (11)$$

where we introduce new notations  $\mathbf{o}_t^M \in \mathcal{S}_t^M$  to avoid confusion with notation  $\mathbf{o}_t^h$ . The likelihood function can be interpreted as representing the probability of success of human detection for an enclosed set of  $M$  particles. Also, it has the same form as the Geometric distribution, and when coupled with the Beta distribution as the conjugate prior, it allows *closed-form* updates of human detection reliability  $a_t^h$ . It will be discussed in Section V.

### C. Sensor Data Fusion

For the likelihood  $p(\mathbf{o}_t | \mathbf{p}_t) = p(\mathbf{o}_t^u, \mathbf{o}_t^h | \mathbf{p}_t)$ , the human-drawing observation and the autonomy observation are aggregated with no exchange of information among team members, as follows:

$$\begin{aligned} p(\mathbf{o}_t^u, \mathbf{o}_t^h | \mathbf{p}_t) &= p(\mathbf{o}_t^u | \mathbf{p}_t) \int_0^1 p(\mathbf{o}_t^h | \mathbf{x}_t, a_t^h; \mathbf{L}) p(a_t^h) da_t^h \\ &= \underbrace{\prod_{u \in \mathcal{U}} p(\mathbf{o}_t^u | \mathbf{p}_t)^{w_u}}_{\text{Autonomous observations}} \underbrace{\prod_{h \in \mathcal{H}} \int_0^1 p(\mathbf{o}_t^h | \mathbf{x}_t, a_t^h; \mathbf{L})^{w_h} p(a_t^h) da_t^h}_{\text{Human-drawing observations}}, \end{aligned} \quad (12)$$

where the weight parameters,  $w_u \in [0, 1] \subseteq \mathbb{R}$  and  $w_h \in [0, 1] \subseteq \mathbb{R}$  that determine the relative trust assigned to each sensor. The weight parameters are subject to the constraint  $\sum w_i = 1$ , ensuring that the total weight remains normalized. We assume independent and identically distributed (i.i.d) conditions for each sensor measurement. The integration term involves marginalization with respect to  $a_t^h$ .

In this paper, we allocate the weights based on the number of autonomous sensors and human operators involved in the system. For example, if there are two autonomous sensors ( $u_n = 2$ ) and one human operator ( $h_m = 1$ ), we assign  $w_{u_1} = w_{u_2} = 2/5$  and  $w_{h_1} = 1/5$ . This weight assignment allows average consensus between autonomous sensors and human operators. By adjusting these weight parameters, we can balance the contribution of each sensor in the multiple sensors system.

## V. JOINT BAYESIAN LEARNING FOR TARGET LOCALIZATION AND HUMAN PARAMETERS

This section introduces a joint Bayesian learning approach for target localization and human parameters estimation, aiming to estimate the joint posterior distribution  $p(\mathbf{p}_t, a_t^h | \mathbf{o}_{1:t})$  conditioned on all measurements. The joint posterior distribution is factorized by

$$p(\mathbf{p}_t, a_t^h | \mathbf{o}_{1:t}) = p(a_t^h | \mathbf{p}_t, \mathbf{o}_{1:t}) p(\mathbf{p}_t | \mathbf{o}_{1:t}), \quad (13)$$

where  $p(\mathbf{p}_t | \mathbf{o}_{1:t})$  is the distribution of the position of the target, and  $p(a_t^h | \mathbf{p}_t, \mathbf{o}_{1:t})$  is the distribution of the human parameter given the target position.

The main idea is to perform recursive updates on the two distributions. First, we update the distribution of the target position given the human parameter. Next, we update the distribution of the human parameter by marginalizing the given distribution of the target position. The mathematical form is given by

$$p(a_t^h | \mathbf{o}_{1:t}) = \int_{\Theta} p(a_t^h | \mathbf{p}_t, \mathbf{o}_{1:t}) p(\mathbf{p}_t | \mathbf{o}_{1:t}) d\mathbf{p}_t. \quad (14)$$

### A. Bayesian Learning for Target Localization

Firstly, the target position is computed from (1) using the transition model (4) and the likelihood model (12) in the finite-state HMM framework. Hence, the distribution of the target position is

$$\begin{aligned} p(\mathbf{p}_t | \mathbf{o}_{1:t}) &= \eta p(\mathbf{o}_t | \mathbf{p}_t) \int_{\Theta} p(\mathbf{p}_t | \mathbf{p}_{t-1}) p(\mathbf{p}_{t-1} | \mathbf{o}_{1:t-1}) d\mathbf{p}_{t-1} \\ &= \eta \prod_{u \in \mathcal{U}} p(\mathbf{o}_t^u | \mathbf{p}_t)^{w_u} \prod_{h \in \mathcal{H}} \int_0^1 p(\mathbf{o}_t^h | \mathbf{x}_t, a_t^h; \mathbf{L})^{w_h} p(a_t^h) da_t^h \\ &\quad \times \int_{\Theta} p(\mathbf{p}_t | \mathbf{p}_{t-1}) p(\mathbf{p}_{t-1} | \mathbf{o}_{1:t-1}, \mathbf{o}_{1:t-1}^h) d\mathbf{p}_{t-1}, \end{aligned} \quad (15)$$

where the integration in the second term can be calculated analytically (see in detail in Appendix A), and  $\eta$  and the integration in the third term can be approximated as a summation. Therefore, the distribution of the target position can result in the form of (2).

### B. Bayesian Learning for Human Parameters

Then, given the posterior distribution of the target position  $p(\mathbf{p}_t | \mathbf{o}_{1:t})$ , the distribution of the human parameter (detection reliability) is updated by

$$\begin{aligned} p(a_t^h | \mathbf{o}_{1:t}) &= \int_{\Theta} p(a_t^h | \mathbf{p}_t, \mathbf{o}_{1:t}) p(\mathbf{p}_t | \mathbf{o}_{1:t}) d\mathbf{p}_t \\ &\propto \int_{\Theta} p(\mathbf{o}_t^h | \mathbf{x}_t, a_t^h; \mathbf{L})^{w_h} p(a_t^h | \alpha_t, \beta_t) p(\mathbf{p}_t | \mathbf{o}_{1:t}) d\mathbf{p}_t \\ &= q_t^s \cdot \text{Beta}(w_h + \alpha_t, w_h(M - 1) + \beta_t) \\ &\quad + (1 - q_t^s) \cdot \text{Beta}(\alpha_t, w_h M + \beta_t), \end{aligned} \quad (16)$$

where  $\propto$  indicates proportionality and the  $q_t^s$  denotes the sum of the weight  $q_t^i$  when  $\mathbf{x}_t^i = \mathbf{o}_t^M$  (i.e.,  $q_t^s = \sum_{\forall \mathbf{x}_t^i = \mathbf{o}_t^M} q_t^i$ ), see in detail in Appendix B. The updated distribution of the human parameter is represented as a weighted sum of two Beta distributions, which, in general, differs from a single Beta distribution [33]. However, when the two

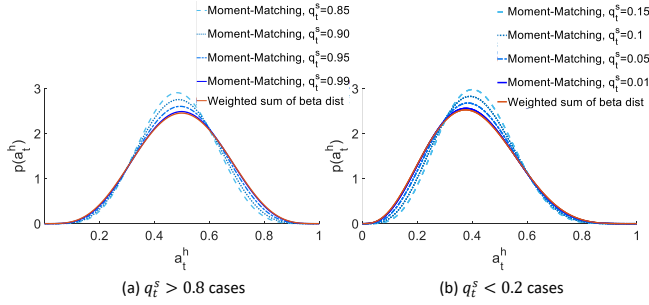


Fig. 5 – Illustration of how the moment-matching result approaches the weighted sum of two Beta distributions.

Beta distributions share identical parameters, the resulting distribution simplifies into a single Beta distribution.

To enhance computation efficiency, we propose using a moment-matching method instead of computationally demanding approaches [25]. To preserve the conjugate prior form, we approximate the weighted sum of two Beta distributions as a single Beta distribution. In practice, since there is a minimal significant difference between the two Beta distributions ( $0 \leq w_h \leq 1$ ), it is highly possible that the weighted sum of two Beta distributions will closely resemble a single Beta distribution.

*Definition 1:* (Conjugate priors [25]) Given a likelihood, conjugate priors allow exact derivation of the posterior distribution and closed-form solutions in which the prior and posterior can be in the same family of distributions.  $\square$

To approximate the resulting distribution of  $p(a_t^h | \mathbf{o}_{1:t})$  as a Beta distribution  $a_t^h \sim \text{Beta}(\alpha_t^*, \beta_t^*)$ , we will employ the first two moments, the mean  $E(a_t^h)$  and variance  $\text{Var}(a_t^h)$ . As a result, we obtain two equations given by:

$$\frac{\alpha_t^*}{\alpha_t^* + \beta_t^*} = \frac{q_t^s \cdot (w_h + \alpha_t) + (1 - q_t^s) \cdot \alpha_t}{w_h M + \alpha_t + \beta_t}, \quad (17)$$

$$\begin{aligned} & \frac{\alpha_t^* \beta_t^*}{(\alpha_t^* + \beta_t^*)^2 \cdot (\alpha_t^* + \beta_t^* + 1)} \\ &= \frac{(q_t^s)^2 \cdot (w_h + \alpha_t) \cdot (w_h(M - 1) + \beta_t)}{(w_h M + \alpha_t + \beta_t)^2 \cdot (w_h M + \alpha_t + \beta_t + 1)} \\ &+ \frac{(1 - q_t^s)^2 \cdot \alpha_t \cdot (w_h M + \beta_t)}{(w_h M + \alpha_t + \beta_t)^2 \cdot (w_h M + \alpha_t + \beta_t + 1)}. \end{aligned} \quad (18)$$

From the two equations (17) and (18), we can compute  $(\alpha_t^*, \beta_t^*)$  numerically. This offers significant advantages in updating human parameters online, enabling real-time target localization.

*Remark 5.1:* The accuracy of the moment-matching method's result relies significantly on  $q_t^s$ . When human operators attentively make accurate drawing observations, the value of  $q_t^s$  notably rises (i.e.,  $q_t^s > 0.8$ ). Conversely, substantial errors by human operators lead to a significant decrease in the value of  $q_t^s$  (i.e.,  $q_t^s < 0.2$ ). As a result, the moment-matching outcomes exhibit a high level of accuracy, see Fig 5.  $\square$

## VI. SIMULATION STUDY

In this section, we assess the effectiveness of our human-autonomy data fusion-based localization algorithm through a simulated scenario. The scenario involves the collaborative

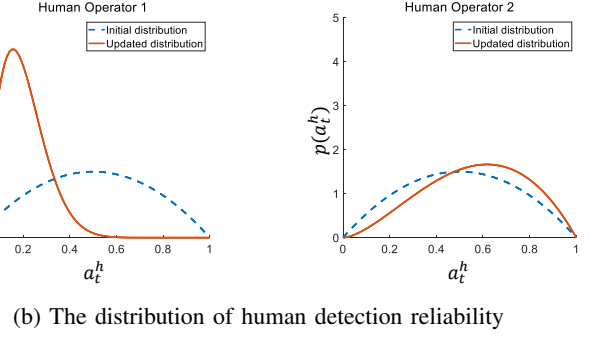
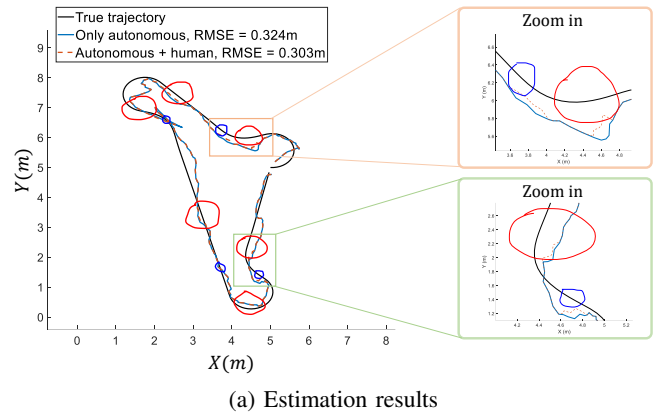


Fig. 6 – The position RMSE and estimated trajectories: (a) shows the position RMSE obtained from estimated trajectories and the human drawing observations. Red human drawings represent contributions from human operator 1, while blue drawings reflect input from human operator 2, (b) shows both the initial distribution and the updated distribution of the human operator's detection reliability.

efforts of three UAVs and two human operators, with the goal of accurately localizing a mobile target. During the simulations, the target is dynamically rendered on the screen, providing a visual representation of its movement. The human operators participate by using a stylus pen to encircle the target's estimated location on the display screen. The simulations are performed within a synthetic environment developed in MATLAB.

### A. Simulation Setting and Parameters

In our simulation scenario, we consider a setup where three UAVs operate at different altitudes: 10, 9, and 8(m). The two human operators involved in the localization task initialize their initial detection reliability, characterized by the same parameters  $a_1^{h1}, a_1^{h2} \sim \text{Beta}(2, 2)$  (i.e., mediocre levels of detection reliability), as indicated by the blue dotted line in Fig 6 (b). The initial position of the target is known a priori. In the transition model, we set  $\sigma_p = 0.5$  (m) and  $\mathbf{v}_0 = [1 \ 1]^T$  (m/s), assuming a homogeneous movement for the target. The autonomous sensor data corresponds to the relative distance between each UAV and the target, with a measurement noise standard deviation of  $\sigma_u = 0.05$  (m), detection probability  $p_d = 0.95$ , and a sampling time of  $T_s = 0.1$  (s). In the discrete sample space, we distribute  $N_p = 400$  particles over the region of interest  $\Theta = [0, 10] \text{ (m)} \times [0, 10] \text{ (m)}$ .

## B. Simulation Results and Discussion

We evaluate the localization accuracy using the root mean squared error (RMSE) metric. The two human operators provide inside drawing observations in our simulation experiments. We are comparing the estimation accuracy of two cases: (1) Only autonomous sensor-based localization, and (2) Autonomous + human sensor fusion. In the “Only autonomous” case, target localization relies solely on data from autonomous sensors, particularly the relative distance information gathered by UAVs. In the “Autonomous + human” case, both autonomous sensors and human drawing observations are combined, taking spatial information into account. Moreover, for the purpose of comparing the update process of human detection reliability distributions, two human operators provide observations on different-sized drawings (large vs small).

Fig. 6 (a) presents the position RMSE as well as a magnified view of the estimated positions corresponding to each human drawing observation. The estimation accuracy is influenced by the observability provided by the relative (range) information collected by UAVs. Despite being less frequent (10 observations) than observations from autonomous sensors, the integration of human drawing data introduces a compensatory mechanism that effectively mitigates estimation errors in the sensors. In Fig. 6 (b), the updated distributions of detection reliability for two human operators are depicted. Human operator 1 experiences diminished reliability due to the larger size of the drawings, even when the observations are accurate. Conversely, human operator 2 benefits from heightened reliability due to the smaller size of the correct drawings. These results effectively reflect detection reliability based on observations. Regarding the moment matching method, we examine the value of  $q_t^s$  throughout the simulations. In this simulation, given the reasonable observations provided by human operators, we can observe that  $q_t^s$  reaches a threshold of at least 0.9995. Consequently, this allows us to derive an accurate updated distribution of human reliability. Within the HMM framework, particle (sample space) quantity and placement significantly impact estimation accuracy and computational efficiency. This can be alleviated by incorporating environmental information, such as maps, or utilizing efficient configuration spaces like probabilistic roadmaps [34].

## VII. CONCLUSIONS

This paper considered human-autonomy collaboration for dynamic target localization in a Bayesian framework. We devised a novel human drawing observation model to provide spatial information, addressing the limitations of autonomous sensors. Specifically, the design of the human drawing observation took into consideration both human detection reliability and inherent uncertainties. With this model, we proposed a joint Bayesian learning approach that encompasses both target localization and dynamic updating of human detection reliability in a computationally efficient manner. Lastly, we demonstrated enhanced target localization outcomes, paralleled by the updated distribution of human detection reliability.

In future work, our focus is on addressing the assumption of non-correlation between sample spaces in human drawing observations. We also plan to undertake modeling efforts to capture the spatial information extracted from the intricate shapes of human drawings. Taking these factors into account,

precise quantification of human observation will improve the accuracy of target localization.

## APPENDIX

### A. Calculation of marginalization for the human likelihood function

The distribution of the target position is

$$\begin{aligned} p(\mathbf{p}_t | \mathbf{o}_{1:t}) &= \eta p(\mathbf{o}_t | \mathbf{p}_t) \int_{\Theta} p(\mathbf{p}_t | \mathbf{p}_{t-1}) p(\mathbf{p}_{t-1} | \mathbf{o}_{1:t-1}) d\mathbf{p}_{t-1} \\ &= \eta \prod_{u \in \mathcal{U}} p(\mathbf{o}_t^u | \mathbf{p}_t)^{w_u} \prod_{h \in \mathcal{H}} \int_0^1 p(\mathbf{o}_t^h | \mathbf{x}_t, a_t^h; \mathbf{L})^{w_h} p(a_t^h) da_t^h \\ &\quad \times \int_{\Theta} p(\mathbf{p}_t | \mathbf{p}_{t-1}) p(\mathbf{p}_{t-1} | \mathbf{o}_{1:t-1}^u, \mathbf{o}_{1:t-1}^h) d\mathbf{p}_{t-1}. \end{aligned} \quad (19)$$

The random variable  $a_t^h \sim \text{Beta}(\alpha_t, \beta_t)$  has a probability density function,

$$f(a_t^h) = \frac{1}{B(\alpha_t, \beta_t)} (a_t^h)^{\alpha_t-1} \cdot (1 - a_t^h)^{\beta_t-1}, \quad (20)$$

where  $a_t^h \in [0, 1] \subseteq \mathbb{R}$ , and  $B(\cdot, \cdot)$  is the Beta function, a normalization constant to ensure that the probability is 1.

Using the Beta probability density function and (11), the second integral term in (19) can be represented by

$$\begin{aligned} &\int_0^1 p(\mathbf{o}_t^h | \mathbf{x}_t, a_t^h; \mathbf{L})^{w_h} p(a_t^h) da_t^h, \\ &= \frac{1}{B(\alpha_t, \beta_t)} \int_0^1 (a_t^h)^{w_h \delta(\mathbf{x}_t, \mathbf{o}_t^M)} \cdot (1 - a_t^h)^{w_h (M - \delta(\mathbf{x}_t, \mathbf{o}_t^M))} \\ &\quad \cdot (a_t^h)^{\alpha_t-1} \cdot (1 - a_t^h)^{\beta_t-1} da_t^h \\ &= \frac{1}{B(\alpha_t, \beta_t)} \int_0^1 (a_t^h)^{w_h \delta(\mathbf{x}_t, \mathbf{o}_t^M) + \alpha_t - 1} \\ &\quad \cdot (1 - a_t^h)^{w_h (M - \delta(\mathbf{x}_t, \mathbf{o}_t^M)) + \beta_t - 1} da_t^h. \end{aligned} \quad (21)$$

By the definition of the Beta function [33], the second integral term in (19) can have analytical form as

$$\begin{aligned} &\int_0^1 p(\mathbf{o}_t^h | \mathbf{x}_t, a_t^h; \mathbf{L})^{w_h} p(a_t^h) da_t^h \\ &= \frac{B(w_h \delta(\mathbf{x}_t, \mathbf{o}_t^M) + \alpha_t, w_h (M - \delta(\mathbf{x}_t, \mathbf{o}_t^M)) + \beta_t)}{B(\alpha_t, \beta_t)}. \end{aligned} \quad (22)$$

### B. The distribution of the human parameter

The distribution of the human parameter can be represented given the distribution of the target position as

$$\begin{aligned} &p(a_t^h | \mathbf{o}_{1:t}) \\ &= \int_{\Theta} p(a_t^h | \mathbf{p}_t, \mathbf{o}_{1:t}) p(\mathbf{p}_t | \mathbf{o}_{1:t}) d\mathbf{p}_t \\ &\propto \int_{\Theta} p(\mathbf{o}_t^h | \mathbf{x}_t, a_t^h; \mathbf{L})^{w_h} p(a_t^h | \alpha_t, \beta_t) p(\mathbf{p}_t | \mathbf{o}_{1:t}) d\mathbf{p}_t \\ &\approx \sum_{i=1}^{N_p} p(\mathbf{o}_t^h | \mathbf{x}_t^i, a_t^h; \mathbf{L})^{w_h} p(a_t^h | \alpha_t, \beta_t) \cdot q_t^i \cdot \delta(\mathbf{L}\mathbf{x}_t - \mathbf{L}\mathbf{x}_t^i), \end{aligned} \quad (23)$$

where  $p(\mathbf{o}_t^h | \mathbf{x}_t^i, a_t^h; \mathbf{L})^{w_h}$  and  $p(a_t^h | \alpha_t, \beta_t)$  show a conjugate prior relationship. Therefore, for given each  $\mathbf{x}_t^i$ , a new Beta distribution can be obtained by

$$\begin{aligned} & p(\mathbf{o}_t^h | \mathbf{x}_t^i, a_t^h; \mathbf{L})^{w_h} p(a_t^h | \alpha_t, \beta_t) \\ & \propto (a_t^h)^{w_h \delta(\mathbf{x}_t^i, \mathbf{o}_t^M) + \alpha_t - 1} \cdot (1 - a_t^h)^{w_h (M - \delta(\mathbf{x}_t^i, \mathbf{o}_t^M)) + \beta_t - 1} \\ & = \text{Beta}(w_h \delta(\mathbf{x}_t^i, \mathbf{o}_t^M) + \alpha_t, w_h (M - \delta(\mathbf{x}_t^i, \mathbf{o}_t^M)) + \beta_t). \end{aligned} \quad (24)$$

Then, using (24), we can represent (23) as a weighted sum of two Beta distributions as given by

$$\begin{aligned} & \sum_{i=1}^{N_p} p(\mathbf{o}_t^h | \mathbf{x}_t^i, a_t^h; \mathbf{L})^{w_h} p(a_t^h | \alpha_t, \beta_t) \cdot q_t^i \cdot \delta(\mathbf{L}\mathbf{x}_t - \mathbf{L}\mathbf{x}_t^i) \\ & = \sum_{i=1}^{N_p} q_t^i \cdot \text{Beta}(w_h \delta(\mathbf{x}_t^i, \mathbf{o}_t^M) + \alpha_t, w_h (M - \delta(\mathbf{x}_t^i, \mathbf{o}_t^M)) + \beta_t) \\ & = \sum_{\forall \mathbf{x}_t^i = \mathbf{o}_t^M} q_t^i \cdot \text{Beta}(w_h + \alpha_t, w_h (M - 1) + \beta_t) \\ & \quad + \left(1 - \sum_{\forall \mathbf{x}_t^i = \mathbf{o}_t^M} q_t^i\right) \cdot \text{Beta}(\alpha_t, w_h M + \beta_t) \\ & = q_t^s \cdot \text{Beta}(w_h + \alpha_t, w_h (M - 1) + \beta_t) \\ & \quad + \left(1 - q_t^s\right) \cdot \text{Beta}(\alpha_t, w_h M + \beta_t). \end{aligned} \quad (25)$$

where  $q_t^s$  denotes the sum of the weight  $q_t^i$  when  $\mathbf{x}_t^i = \mathbf{o}_t^M$  (i.e.,  $q_t^s = \sum_{\forall \mathbf{x}_t^i = \mathbf{o}_t^M} q_t^i$ ).

## REFERENCES

- [1] M. Stachura and E. W. Frew, "Cooperative target localization with a communication-aware unmanned aircraft system," *Journal of Guidance, Control, and Dynamics*, vol. 34, no. 5, pp. 1352–1362, 2011.
- [2] A. Nagaty, C. Thibault, M. Trentini, and H. Li, "Probabilistic cooperative target localization," *IEEE Transactions on Automation Science and Engineering*, vol. 12, no. 3, pp. 786–794, 2015.
- [3] C. Robin and S. Lacroix, "Multi-robot target detection and tracking: taxonomy and survey," *Autonomous Robots*, vol. 40, no. 4, pp. 729–760, 2016.
- [4] T. Kaupp, B. Douillard, F. Ramos, A. Makarenko, and B. Upcroft, "Shared environment representation for a human-robot team performing information fusion," *Journal of Field Robotics*, vol. 24, no. 11–12, pp. 911–942, 2007.
- [5] W. G. Kennedy, M. D. Bugajska, M. Marge, W. Adams, B. R. Fransen, D. Perzanowski, A. C. Schultz, and J. G. Trafton, "Spatial representation and reasoning for human-robot collaboration," in *AAAI*, vol. 7, pp. 1554–1559, 2007.
- [6] L. Burks, I. Lofgren, L. Barbier, J. Muesing, J. McGinley, S. Vunnam, and N. Ahmed, "Closed-loop bayesian semantic data fusion for collaborative human-autonomy target search," in *2018 21st International Conference on Information Fusion (FUSION)*, pp. 2262–2269, IEEE, 2018.
- [7] J. Muesing, N. Ahmed, L. Burks, M. Iuzzolino, and D. Albers Szafir, "Fully bayesian human-machine data fusion for robust online dynamic target characterization," *Journal of Aerospace Information Systems*, vol. 18, no. 2, pp. 26–49, 2021.
- [8] D. L. Hall and J. M. Jordan, *Human-centered information fusion*. Artech House, 2010.
- [9] T. B. Sheridan, T. B. Sheridan, K. Maschinenbauingenieur, T. B. Sheridan, and T. B. Sheridan, *Humans and automation: System design and research issues*, vol. 280. Human Factors and Ergonomics Society Santa Monica, CA, 2002.
- [10] A. Farhadi and J. Redmon, "Yolov3: An incremental improvement," in *Computer vision and pattern recognition*, vol. 1804, pp. 1–6, Springer Berlin/Heidelberg, Germany, 2018.
- [11] M. Brenner, N. Hawes, J. D. Kelleher, and J. L. Wyatt, "Mediating between qualitative and quantitative representations for task-orientated human-robot interaction," in *IJCAI*, pp. 2072–2077, 2007.
- [12] L. Kunze, K. K. Doreswamy, and N. Hawes, "Using qualitative spatial relations for indirect object search," in *2014 IEEE international conference on robotics and automation (ICRA)*, pp. 163–168, IEEE, 2014.
- [13] R. M. Robinson, H. Lee, M. J. McCourt, A. R. Marathe, H. Kwon, C. Ton, and W. D. Nothwang, "Human-autonomy sensor fusion for rapid object detection," in *2015 IEEE/RSJ International Conference on Intelligent Robots and Systems (IROS)*, pp. 305–312, IEEE, 2015.
- [14] H. Cai and Y. Mostofi, "Human-robot collaborative site inspection under resource constraints," *IEEE Transactions on Robotics*, vol. 35, no. 1, pp. 200–215, 2018.
- [15] M. Pavliv, F. Schiano, C. Reardon, D. Floreano, and G. Loianno, "Tracking and relative localization of drone swarms with a vision-based headset," *IEEE Robotics and Automation Letters*, vol. 6, no. 2, pp. 1455–1462, 2021.
- [16] D. C. Shah and M. E. Campbell, "A qualitative path planner for robot navigation using human-provided maps," *The International Journal of Robotics Research*, vol. 32, no. 13, pp. 1517–1535, 2013.
- [17] N. Ahmed, M. Campbell, D. Casbeer, Y. Cao, and D. Kingston, "Fully bayesian learning and spatial reasoning with flexible human sensor networks," in *Proceedings of the ACM/IEEE Sixth International Conference on Cyber-Physical Systems*, pp. 80–89, 2015.
- [18] L. Burks, H. M. Ray, J. McGinley, S. Vunnam, and N. Ahmed, "Harps: An online pomdp framework for human-assisted robotic planning and sensing," *IEEE Transactions on Robotics*, 2023.
- [19] J. Guo, X. Li, Z. Lv, Y. Yang, and L. Li, "Design of real-time video transmission system for drone reliability," in *IOP Conference Series: Materials Science and Engineering*, vol. 790, p. 012004, IOP Publishing, 2020.
- [20] J. Sun, B. Li, Y. Jiang, and C.-y. Wen, "A camera-based target detection and positioning uav system for search and rescue (sar) purposes," *Sensors*, vol. 16, no. 11, p. 1778, 2016.
- [21] B. Rudic, M. Pichler-Scheder, R. Schmidt, C. Helm, D. Efrosinin, C. Kastl, and W. Auer, "A geometry-aware hidden markov model for indoor positioning," in *2020 IEEE/ASME International Conference on Advanced Intelligent Mechatronics (AIM)*, pp. 547–552, IEEE, 2020.
- [22] H.-J. Yoon, D. Lee, and N. Hovakimyan, "Hidden markov model estimation-based q-learning for partially observable markov decision process," in *2019 American Control Conference (ACC)*, pp. 2366–2371, IEEE, 2019.
- [23] U. Rosolia, D. C. Guastella, G. Muscato, and F. Borrelli, "Model predictive control in partially observable multi-modal discrete environments," *IEEE Control Systems Letters*, 2023.
- [24] A. Papoulis and S. Unnikrishna Pillai, *Probability, random variables and stochastic processes*. McGraw-Hill Europe, 2002.
- [25] M. Svensén and C. M. Bishop, "Pattern recognition and machine learning," 2007.
- [26] A. Bewley, Z. Ge, L. Ott, F. Ramos, and B. Upcroft, "Simple online and realtime tracking," in *2016 IEEE international conference on image processing (ICIP)*, pp. 3464–3468, IEEE, 2016.
- [27] N. Wojke, A. Bewley, and D. Paulus, "Simple online and realtime tracking with a deep association metric," in *2017 IEEE international conference on image processing (ICIP)*, pp. 3645–3649, IEEE, 2017.
- [28] N. L. Baisa and A. Wallace, "Development of a n-type gm-phd filter for multiple target, multiple type visual tracking," *Journal of Visual Communication and Image Representation*, vol. 59, pp. 257–271, 2019.
- [29] M. Tan, R. Pang, and Q. V. Le, "Efficientdet: Scalable and efficient object detection," in *Proceedings of the IEEE/CVF conference on computer vision and pattern recognition*, pp. 10781–10790, 2020.
- [30] Z. Cai and N. Vasconcelos, "Cascade r-cnn: Delving into high quality object detection," in *Proceedings of the IEEE conference on computer vision and pattern recognition*, pp. 6154–6162, 2018.
- [31] R. Hartley and A. Zisserman, *Multiple view geometry in computer vision*. Cambridge university press, 2003.
- [32] I. Arous, L. Dolamic, J. Yang, A. Bhardwaj, G. Cuccu, and P. Cudré-Mauroux, "Marta: Leveraging human rationales for explainable text classification," in *Proceedings of the AAAI conference on artificial intelligence*, vol. 35, pp. 5868–5876, 2021.
- [33] D. Wackerly, W. Mendenhall, and R. L. Scheaffer, *Mathematical statistics with applications*. Cengage Learning, 2014.
- [34] A. Bachrach, S. Prentice, R. He, P. Henry, A. S. Huang, M. Krainin, D. Maturana, D. Fox, and N. Roy, "Estimation, planning, and mapping for autonomous flight using an rgb-d camera in gps-denied environments," *The International Journal of Robotics Research*, vol. 31, no. 11, pp. 1320–1343, 2012.